Using A Physics-informed State-space Model to Assess Future Projection Uncertainty of Regional Climate and Water Supply

Yuchuan Lai
Research Engineer, Tetra Tech Inc., Lafayette CA, USA
Previous affiliation: Postdoctoral Research Associate, Department of Civil and Environmental Engineering, Carnegie Mellon University, Pittsburgh PA, USA

Matteo Pozzi
Professor, Department of Civil and Environmental Engineering, Carnegie Mellon University, Pittsburgh PA, USA

ABSTRACT: A state-space model (SSM) integrating physical parameters is proposed and developed in this work, to describe the increase of global average temperature and the subsequent changes in regional climate and hydrology. This SSM approach aims at providing updated and improved forecasts, based on observations and using Bayesian inference, and at facilitating flexible engineering decision-making schemes. Global climate model simulations are used for informing the distribution of the parameters of the SSM. The case study of the Colorado River Basin serves as a preliminary application of the method, to forecast changes in the upper basin natural flow. The method projects that the post-2000 low flow volume will continue, or become even lower on average, although such projections are subject to large uncertainty. Given the increasing need of climate projections in the design, operation, and management of infrastructure, the SSM approach can serve as a useful tool, informed by historical records, to facilitate engineering applications.

1. INTRODUCTION

An increasingly important task for civil engineers is to design, operate, and manage infrastructure with adequate adaptation and resilience to the changing climate (ASCE-CACC 2015), given the growing impacts of climate change, such as climate extremes (ASCE Task Committee on Future Weather and Climate Extremes 2021). One impacted sector that of is water resource, which faces a number of challenges related to droughts (e.g., Lukas and Payton 2020) and as well as heavy rainfall events and subsequent flood controls (Drum et al. 2017).

Forecasts of regional climate and hydrology can help assessing the reliability of long-term water supply and subsequently risks and adaptation policies needed, although such projections are subject to various sources of uncertainty (Lai et al. 2022). An approach to address future projection uncertainty and to facilitate decision-making is to adopt a flexible assessment and planning scheme (Herman et al., 2020; Ribes et al., 2021), by utilizing observations over time to reduce uncertainty.

The objective of this work is to develop a physics-informed, probabilistic time series model to obtain future projections of regional climate and hydrology conditional on observations and to facilitate regional water resource management. The proposed state-space model (SSM) forecasts changes of global average temperature, regional climate and hydrology, it relies on physical parameters to inform the data analysis, and it can be updated with new observations.

The SSM is implemented in the investigation of the Colorado River Basin, in a preliminary manner, to forecast regional water supply. The Colorado River Basin is currently facing a basin-wide water supply crisis (Wheeler et al. 2022), and heavy policy interventions, such as substantial water supply cuts, are likely needed. By using the proposed SSM, this application aims at updating and evaluating future projected water supply, given the drought conditions experienced starting from the year 2000 (Lukas and Payton 2020).

This paper is organized as follows: the method of the proposed SSM is discussed in the subsequent Section 2, the application of the SSM to the Colorado River Basin and the obtained results are discussed in Section 3, and some general findings and conclusions on the proposed SSM are offered in Section 4.

2. METHODOLOGY

The proposed SSM consists of two components: one models changes in global average temperature, and one models changes in regional climate and hydrology. Using the Kalman filter and the maximum a posteriori (MAP) estimation method, global climate model (GCM) simulations and historical observations are processed, to obtain posterior distributions of the parameters to update future projections. These components of the SSM are discussed in the following sections.

2.1. An energy balance model for the global average temperature

The modeling of global temperature response to increasing greenhouse gas concentrations and other internal and external forcings is developed based on two-layer energy balance scheme (Cummins et al. 2020). This two-layer model describes the temperature responses (temperature anomalies) of surface (including surface air and swallow ocean) and deep ocean layers at time t to the imposed forcings F (i.e. factors contributing to temperature increase such as greenhouse gas, GHG, concentrations) as:

$$\begin{aligned} C_1 \frac{\mathrm{d}T}{\mathrm{d}t} &= F - \lambda T - \beta(T - T_{\mathrm{LO}}) \\ C_2 \frac{\mathrm{d}T_{\mathrm{LO}}}{\mathrm{d}t} &= \beta(T - T_{\mathrm{LO}}) \end{aligned} \tag{1}$$

where T and T_{LO} are the temperature anomalies at the surface layer and at the deep ocean (i.e., Lower Ocean) layer, respectively; λ is the climate feedback parameter; C_1 and C_2 are the heat capacity parameters for the two layers; and β is the heat exchange coefficient.

By applying an approximate solution to Eq.(1), a state-space representation can be obtained, which consists of a state variable matrix $\mathbf{x}(t)$ as true temperature of surface and deep ocean temperature at year t:

$$\begin{aligned} \mathbf{x}(t+1) &= \mathbf{A}\mathbf{x}(t) + \mathbf{B}\mathbf{F}(t) + \boldsymbol{\omega}(t) \\ \mathbf{x}(t) &= \begin{bmatrix} T(t) & T_{\mathrm{LO}}(t) \end{bmatrix}^{\intercal} \\ \mathbf{A} &= \begin{bmatrix} 1 - \frac{\lambda}{C_1} - \frac{\beta}{C_1} & \frac{\beta}{C_1} \\ \frac{\beta}{C_2} & 1 - \frac{\beta}{C_2} \end{bmatrix} \\ \mathbf{B} &= \frac{1}{C_1} \begin{bmatrix} \gamma_1 & \gamma_2 & 1 \\ 0 & 0 & 0 \end{bmatrix} \\ \mathbf{F}(t) &= \begin{bmatrix} F_{(t)}^{\mathrm{GHG}} & F_{(t)}^{\mathrm{aerosol}} & F_{(t)}^{\mathrm{other}} \end{bmatrix}^{\intercal} \\ \boldsymbol{\omega}(t) &= \begin{bmatrix} \omega_1(t) & \omega_2(t) \end{bmatrix}^{\intercal} \end{aligned} \tag{2}$$

where γ_1 and γ_2 are two linear scaling coefficients to consider the uncertainty related to the forcings of greenhouse gases and aerosols; and ω_1 and ω_2 are two coefficients for white noise of surface and deep ocean temperature.

The surface-layer temperature is subsequently modeled with a output function (measurements of deep ocean temperature are omitted in this work to simplify calculations, although they can be included by adjusting output matrix $\mathbf{D}$):

$$y(t) = \mathbf{D}\mathbf{x}(t) + v(t); \quad \mathbf{D} = \begin{bmatrix} 1 & 0 \end{bmatrix} \tag{3}$$

where $y(t)$ is the measured global average surface temperature at year t and $v(t)$ is white noise at year t, independent of $\boldsymbol{\omega}(t)$.

Eq.(2) and (3) constitute a state-space representation of changes in global average temperature. The other component of the SSM relates the global average temperature to changes in regional climatic and hydrological variables.

2.2. Model of regional climate and hydrology

The modeling of regional climate and hydrology is achieved by introducing additional scaling and correlation factors to relate the changes in global average temperature to changes in regional temperature, precipitation and hydrology. This use of scaling factors for modeling regional climate change is consistent with a pattern scaling approach (Tebaldi and Arblaster 2014). Similarly, the effect of regional temperature and precipitation on hydrology such as streamflow is simplified assuming a linear correlation, in this work, similarly to temperature

sensitivity and precipitation elasticity when assessing natural flow of the Colorado River Basin (Vano and Lettenmaier 2014).

The simplified regional equations therefore are:

$$T_r = k_1 T; \quad P_r = k_2 T; \quad H_r = l_1 T_r + l_2 P_r \tag{4}$$

where T_r, P_r, and H_r are the changes of regional temperature, precipitation, and hydrology; k_1 and k_2 are the two scaling factors for regional temperature and precipitation; and l_1 and l_2 are the two correlation coefficients describing the impacts of regional temperature and precipitation changes on regional hydrology.

Eq.(4) is then developed into an output function, similar to Eq.(3). However, regional temperature and precipitation often exhibit strong autocorrelation (Lai and Dzombak 2019) and thus we adopt autocorrelated noise terms for the regional output function, which is:

$$\begin{aligned}
\boldsymbol{y}(t) &= \mathbf{D}\mathbf{x}(t) + \boldsymbol{\delta}(t) \\
\boldsymbol{\delta}(t+1) &= \boldsymbol{\rho}\,\boldsymbol{\delta}(t) + \boldsymbol{\nu}(t) \\
\boldsymbol{y}(t) &= \begin{bmatrix} y(t) & y_{tr}(t) & y_{pr}(t) & y_{hr}(t) \end{bmatrix}^\intercal \\
\mathbf{D} &= \begin{bmatrix} 1 & 0 & 0 \\ 0 & 1 & 0 \\ 0 & 0 & 1 \\ 0 & l_1 & l_2 \end{bmatrix} \begin{bmatrix} 1 & 0 \\ k_1 & 0 \\ k_2 & 0 \end{bmatrix} \\
\boldsymbol{\rho} &= \begin{bmatrix} 0 & 0 & 0 & 0 \\ 0 & \rho_{tr} & 0 & 0 \\ 0 & 0 & \rho_{pr} & 0 \\ 0 & (\rho_{tr}-\rho_{hr})l_1 & (\rho_{pr}-\rho_{hr})l_2 & \rho_{hr} \end{bmatrix} \\
\boldsymbol{\nu}(t) &= \begin{bmatrix} \nu(t) & \nu_{tr}(t) & \nu_{pr}(t) & \nu_{hr}(t) \end{bmatrix}^\intercal
\end{aligned} \tag{5}$$

where $y_{tr}(t)$, $y_{pr}(t)$, and $y_{hr}(t)$ are the changes in regional temperature, precipitation, and hydrology at year t; $\delta_{tr}(t)$, $\delta_{pr}(t)$, and $\delta_{hr}(t)$ are the noises at year t (note that noise of hydrology includes the correlated noise of regional temperature and precipitation); ρ_{tr}, ρ_{pr}, and ρ_{hr} are the respective correlation coefficients; and $\nu_{tr}(t)$, $\nu_{pr}(t)$, and $\nu_{hr}(t)$ are independent white noises.

The parameters in Eq.(5) (e.g., k_1, k_2, l_1, and l_2) are assumed to be independent of the parameters describing the global average temperature in the previous Section 2.1. The computation of posterior distributions for the parameters in Section 2.1 and for the parameters in this section are therefore separately conducted, as further discussed in Sections 2.4 and 2.5.

2.3. Applying Kalman filter and MAP

A procedure based on the Kalman filter and the MAP estimator is applied to obtain the posteriors distributions (Giordani et al. 2011). However, instead of directly applying the SSM to process historical observations with priors identified from literature, GCM simulations – representing scenarios of global and regional climate evaluations – are first processed, to obtain parameter posterior distributions, which subsequently serve as the prior to process historical observations. The processing of GCM simulations and historical observations therefore constitute a two-step approach (discussed in the subsequent sections), and both steps share a same procedure of using the Kalman filter and the MAP estimator.

Applying the Kalman filter and the MAP estimator relies using different sets of parameter values during each iterations, calculating the likelihood function of parameter values using Kalman filter, maximizing the product of likelihood and prior distributions using the L-BFGS-B algorithm (Byrd et al. 1995), and applying the Laplace approximation based on the Hessian matrix, to estimate the posterior distribution. Further details can be found in Nocedal and Wright (2006) and Barber (2011).

2.4. Processing GCM simulations

Each GCM simulation is considered as a realization of the (global and regional) climate evolution. By processing GCM simulations with the SSM, we aims at identifying a reasonable prior distribution for analyzing the historic data (e.g., understanding the correlation among the parameters).

Individual GCM simulations are processed using the SSM to obtain approximated Gaussian posteriors:

$$\boldsymbol{\Theta}_i | \mathbf{Y}_i \overset{\text{approx}}{\sim} \mathcal{N}(\boldsymbol{\Theta}_i, \hat{\boldsymbol{\mu}}_i, \hat{\boldsymbol{\Sigma}}_i) \tag{6}$$

where $\boldsymbol{\Theta}_i$ contains the SSM parameters for GCM i, $\mathbf{Y}_i$ is refers to the simulated data from GCM i,

and $\hat{\boldsymbol{\mu}}_i$ and $\hat{\boldsymbol{\Sigma}}_i$ are the approximated posterior mean vector and covariance matrix for GCM i.

As previously mentioned, the parameters describing changes in regional climate and hydrology are considered as independent from the parameters describing global average temperature, the processing of GCM simulations consequently involves two separate steps. The first step is to process GCM simulations of global average temperature to obtain posterior distributions for the parameters described in Section 2.1, whereas the second step is to include additional GCM simulations of regional temperature, precipitation, and hydrology to obtain the regional parameters described in Section 2.2 (mean values for the parameters obtained in the first step are used, when appropriate).

2.5. Updating forecasts based on historical observations

Historical observations are used in this step, along with the prior distribution derived from the previous processing of GCM simulations. This step of obtaining the derived priors can be summarized as:

$$\begin{gathered}\boldsymbol{\Theta}|\mathbf{Y} \overset{\text{approx}}{\sim} \mathcal{N}(\hat{\boldsymbol{\mu}}, \hat{\boldsymbol{\Sigma}}) \\ p(\boldsymbol{\Theta}|\mathbf{Y}) \simeq \sum_{i=1}^{m} f_i(\boldsymbol{\Theta}) p(\mathrm{M}_i); \quad f_i(\boldsymbol{\Theta}_i) = p(\boldsymbol{\Theta}_i|\mathbf{Y}_i) \\ \hat{\boldsymbol{\mu}} = \sum_{i=1}^{m} p(\mathrm{M}_i)\hat{\boldsymbol{\mu}}_i \quad \hat{\boldsymbol{\Sigma}} = \sum_{i=1}^{m} p(\mathrm{M}_i)[\hat{\boldsymbol{\Sigma}}_i + (\hat{\boldsymbol{\mu}}_i - \hat{\boldsymbol{\mu}})(\hat{\boldsymbol{\mu}}_i - \hat{\boldsymbol{\mu}})^\top]\end{gathered} \tag{7}$$

where $\mathbf{Y}$ represents all the GCM simulations, $\hat{\boldsymbol{\mu}}$ and $\hat{\boldsymbol{\Sigma}}$ are the combined posterior mean and variance matrices from different GCMs (further used as derived priors), and $p(\mathrm{M}_i)$ is the probability of GCM i (these probabilities are assumed to be the same for all GCMs).

Using the derived priors and the SSM, historical observations ($\mathbf{y}_h$) are subsequently processed using the Kalman filter and MAP approach described in Section 2.3. Similar to the processing of GCM simulations, the posterior distributions of the parameter describing the global average temperature (in Section 2.1) and of the parameters of modeling regional climate and hydrology (in Section 2.2) are separately obtained.

After the posterior distributions $p(\boldsymbol{\Theta}|\mathbf{Y}, \mathbf{y}_h)$ are obtained, the updated forecasts are generated based on the total probability formula:

$$p(\boldsymbol{y}^*|\mathbf{Y}, \boldsymbol{y}_h) = \int p(\boldsymbol{y}^*|\boldsymbol{\Theta}, \mathbf{y}_h) p(\boldsymbol{\Theta}|\mathbf{Y}, \mathbf{y}_h) \mathrm{d}\boldsymbol{\Theta} \tag{8}$$

where $\boldsymbol{y}^*$ is the future time series and $p(\boldsymbol{y}^*|\mathbf{Y}, \mathbf{y}_h)$ is the updated, future projections based on historical observations.

In this case, a Monte Carlo sampling approach is used for Eq.(8) to obtain the updated projections. The steps include randomly selecting parameter values from the posterior distribution $p(\boldsymbol{\Theta}|\mathbf{Y}, \mathbf{y}_h)$, fitting the time series of historical observations $\mathbf{y}_h$ using the Kalman filter and the sampled parameter values, projecting future climate, and integrating results from a large number of samples.

This proposed SSM is applied to the study of the Colorado River Basin, which is discussed in the subsequent Section 3.

3. APPLICATION TO THE COLORADO RIVER BASIN

Communities in the Colorado River Basin are experiencing a prolonged drought since 2000, and the regional water supply faces increasing pressures and challenges (Lukas and Payton 2020). A map of Colorado River Basin can be found in Figure 1. The upper basin provides around 92% of water supply (Lukas and Payton 2020) to the whole basin, and thus an assessment on the natural flow of the upper basin is conducted in this work. Specifically, natural flow estimated at Lees Ferry – a key indicator of regional water supply – is assessed, along with the average temperature and precipitation for the upper basin. The natural flow at Lees Ferry was estimated to be 17.5 million acre-feet (MAF) per year during the negotiation on water allocations in 1922, while the average natural flow of 20$^{\text{th}}$ century was around 15.2 MAF/year and decreased to 12.3 MAF/year after 2000 (Wheeler et al. 2022), resulted in various water shortages and cuts in the region.

3.1. Data

Historical observations used in this work include the global average temperature, the average temperature and the total precipitation for the upper basin,

Figure 1: The map of the upper and lower Colorado River Basin. The annual average temperature and precipitation of the upper basin and natural flow at Lees Ferry of Colorado River – representing the total upper basin natural flow – are assessed in this work.

and the natural flow estimated at Lees Ferry. These time series of temperature, precipitation, and natural flows are obtained from NOAA (2022) and Bureau of Reclamation (2022) and represent the different water years (October 1st to September 30th) starting from 1881 (for temperature and precipitation) and 1906 (for natural flow).

GCM simulations of global average temperature, upper basin average temperature, total precipitation, and runoff volumes are obtained. The temperature, precipitation, and runoff volumes for the upper basin are area-averaged downscaled GCM simulations (using the localized constructed analog downscaling; Pierce et al. 2014) and simulation output from further using the variable infiltration capacity model (for natural flow; total upper basin flow is obtained by calculating the product of total area and areal averaged flow volumes). These results were obtained from LLNL (2022). GCMs of Coupled Model Intercomparison Project Phase 5 (CMIP5) are used along with corresponding forcing time series (Meinshausen et al. 2011). The GCMs of CMIP5 are used because of the limited downscaling results from the GCMs of recent CMIP6. For processing of historical observations, the forcing time series are obtained from IPCC sixth assessment report (Smith et al. 2021) and represent the recent Shared Socioeconomic Pathway (SSP) scenarios (Meinshausen et al., 2020).

3.2. Updated forecasts from SSM

Following the procedures based on the SSM described in the previous sections, the projected changes in global average temperature, upper basin average temperature, total precipitation, and annual natural flow are obtained. The results are presented in Figure 2. In addition to the use of all available historical observations up to 2022, a comparison of projection results using the historical observations up to 1992 is also provided in Figure 2.

Comparing the two forecasts in Figure 2, we note that the use of additional observations results in some changes in the projected global temperature and in the upper basin temperature and precipitation. The end-of-century mean projection for global average temperature anomaly under SSP5-8.5, for example, reduces from around 5ºC to 4.5ºC when additional 30 years of observations are used. The projected temperature for the upper basin also moderately reduces, whereas the upper basin precipitation is projected with a slightly decreasing trend.

The projected natural flow in Figure 2 highlights the challenges of the current and future regional water supply at Colorado River Basin. According to the results, the mean projected natural flow is likely to stay below the 12.3 MAF/year (a post-2000 average), with a possible further reduction. Notably, the projected natural flow does not exhibit observable changes when additional 30-year observations are used, which is likely because the upper basin temperature is projected with a moderately less increasing trend, offsetting the projected slightly decreasing precipitation trend. It should also be noted that, the projected natural flow is subject to large annual variability, e.g., the 95% confidence intervals exhibit a range of more than 12.5 MAF/year (upper minus lower bound).

Reduction of projection uncertainty with additional

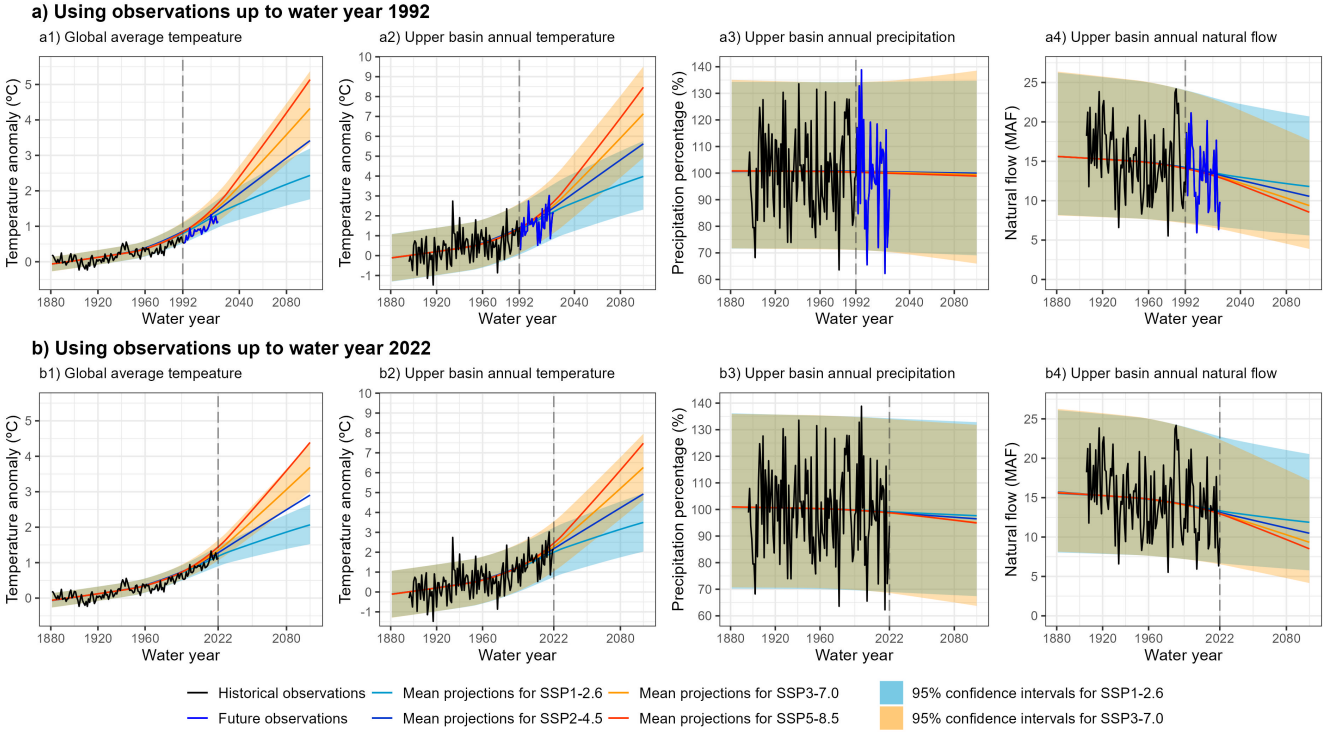

Figure 2: Updated probablistic projections of global average temperature and temperature, precipitation, and natural flow of the upper Colorado River Basin conditional on historical observations. The anomalies are calculated based on the first 30-year averages. As a sampling and simulation procedure is used to obtain future projections, the LOESS smoothing (Cleveland 1979) is applied to projected means and 95% confidence intervals.

observations is more evident in the global and regional temperature series in Figure 2. The results of projection uncertainty for global average temperature are consistent with the previous studies, e.g., Ribes et al. (2021) suggests that the end-of-century SSP2-4.5 and SSP5-8.5 projections of global average temperature are around 2.3-3.7°C and 3.8-6.0°C (90% confidence intervals), respectively. When additional 30 years of observations are processed in Figure 2, we note a limited reduction of the uncertainty on the precipitation and the natural flow, which is likely because of the large internal variability of these two series.

3.3. Posterior distributions of regional parameters

To further assess regional climate change and implications on regional water supply, further analyses on the key regional parameters are conducted. The objective is to assess posterior probabilities based on an increasing amount of observations.

The results of parameter posterior probabilities calculated from four SSM parameters (k_1, k_2, l_1, and l_2) are presented in Figure 3. Corresponding to these individual SSM parameters, the distributions of the commonly assessed coefficients, e.g., the temperature sensitivity and precipitation elasticity of annual upper basin natural flow (Vano and Lettenmaier 2014), are presented,

As shown in Figure 3, with additional observations the parameter uncertainty can be reduced, although such reductions depends on the specific parameter. The temperature scaling factor k_1 exhibits a greater reduction of uncertainty, while the other three parameters have a limited reduction.

The results of temperature sensitivity and precipitation elasticity of natural flow (calculated from l_1 and l_2) in Figure 3 are generally consistent with the results from previous studies although, some differences exist. For example, by using hydrological models, Vano and Lettenmaier (2014) suggests an average temperature sensitivity value of -6.5%/°C and a precipitation elasticity value of 2.2%/%. Ho-

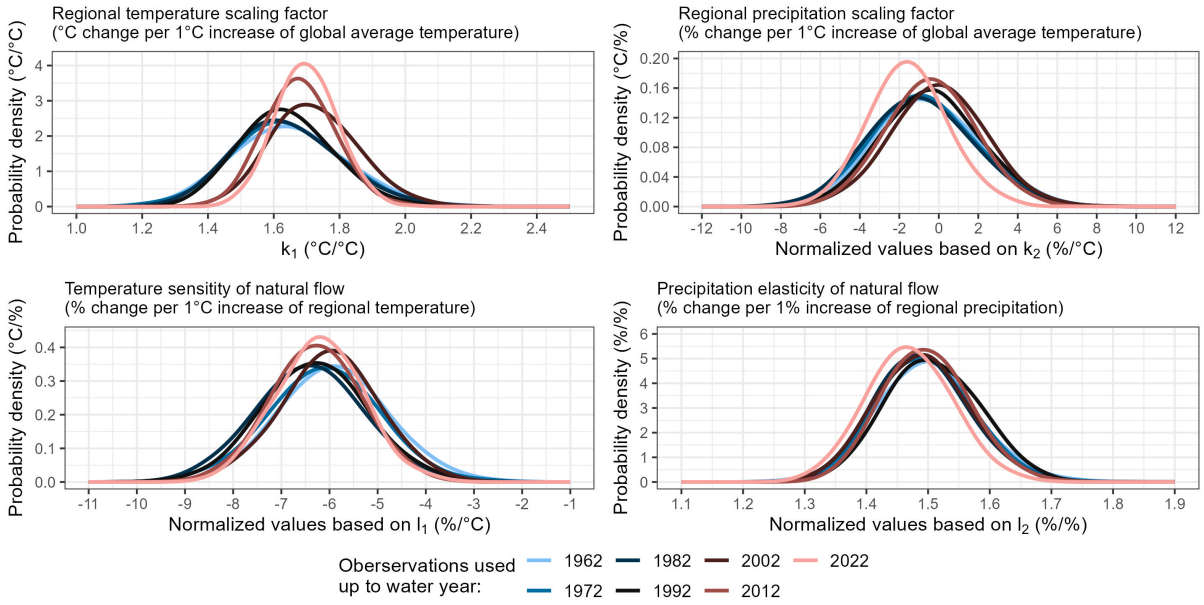

Figure 3: Parameter poserior probability densities when a different amount of observations are processed. Distributions of k_2, l_1, and l_2 are converted to commonly used coefficient values.

erling et al. (2019) shows a result of -2.5%/°C and 2%/%, respectively.

4. CONCLUSIONS

On the basis of a energy balance model, a SSM is proposed and developed in this work, to describe the increase of global average temperature and consequent changes in regional climate and hydrology. This SSM approach integrates the results from GCM simulations, and provides updated and improved projections based on historical observations in order to support flexible engineering decision-making. The observation-based projections and the parameter posterior probabilities can contribute to the assessment of regional climate and of water supply. For example, the projections of natural flow for the upper Colorado River Basin confirm and highlight the regional water supply challenges, suggesting that the post-2000 low flow conditions is likely to continue in the future (on average).

In terms of reduction of projection uncertainty, the results suggest that such reductions depend on the particular regional time series assessed. For the precipitation and natural flow series, the reduction of uncertainty is limited, likely because of the relatively large internal variability.

Further development on the SSM can be made, including a non-linear modeling of regional climate (in response to global average temperature) and a tailored approach for a particular region and hydrological variables. Given that infrastructure resilience to climate change is increasingly important, the use of this SSM approach can help supporting engineering analysis and decision-making.

ACKNOWLEDGEMENT

The research is supported by the National Science Foundation (NSF), grants CMMI #1663479 "From Future Learning To Current Action: Long-Term Sequential Infrastructure Planning Under Uncertainty" and SES #1919453 "Attitude towards information in multi-agent settings: Understanding and mitigating Avoidance and Over-Evaluation".

REFERENCES

ASCE-CACC (2015). "Adapting Infrastructure and Civil Engineering Practice to a Changing Climate." *Report no.*, ASCE.

ASCE Task Committee on Future Weather and Climate Extremes (2021). *Impacts of Future Weather and Climate Extremes on United States Infrastructure: Assessing and Prioritizing Adaptation Actions*. American Society of Civil Engineers - Committee on Adaptation to a Changing Climate, Reston, Virginia.

Barber, D. (2011). "Bayesian Reasoning and Machine Learning." *Bayesian Reasoning and Machine Learning*.

Bureau of Reclamation (2022). "Colorado River Basin Natural Flow and Salt Data, <https://www.usbr.gov/lc/region/g4000/NaturalFlow/current.html>.

Byrd, R., Lu, P., Nocedal, J., and Zhu, C. (1995). "A limited memory algorithm for bound constrained optimization." *Journal of Scientific Computing*, 16(5), 1190–1208.

Cleveland, W. S. (1979). "Robust locally weighted regression and smoothing scatterplots." *Journal of the American statistical association*, 74(368), 829–836.

Cummins, D. P., Stephenson, D. B., and Stott, P. A. (2020). "Optimal estimation of stochastic energy balance model parameters." *Journal of Climate*, 33(18), 7909–7926.

Drum, R. G., Noel, J., Kovatch, J., Yeghiazarian, L., Stone, H., Stark, J., Kirshen, P., Best, E., Emery, E., Trimboli, J., Arnold, J., and Raff, D. (2017). "Ohio River Basin - Formulating Climate Change Mitigation/Adaptation Strategies through Regional Collaboration with the ORB Alliance." *Report no.*, U.S. Army Corps of Engineers, Institute for Water Resources: Alexandria, VA.

Giordani, P., Pitt, M., and Kohn, R. (2011). "Bayesian inference for time series state space models." *The Oxford Handbook of Bayesian Econometrics*.

Herman, J. D., Quinn, J. D., Steinschneider, S., Giuliani, M., and Fletcher, S. (2020). "Climate Adaptation as a Control Problem: Review and Perspectives on Dynamic Water Resources Planning Under Uncertainty." *Water Resources Research*, 56(2).

Hoerling, M., Barsugli, J., Livneh, B., Eischeid, J., Quan, X., and Badger, A. (2019). "Causes for the century-long decline in Colorado River flow." *Journal of Climate*, 32(23), 8181–8203.

Lai, Y. and Dzombak, D. A. (2019). "Use of Historical Data to Assess Regional Climate Change." *Journal of Climate*, 32(14), 4299–4320.

Lai, Y., Lopez-Cantu, T., Dzombak, D. A., and Samaras, C. (2022). "Framing the Use of Climate Model Projections in Infrastructure Engineering: Practices, Uncertainties, and Recommendations." *Journal of Infrastructure Systems*, 28(3), 1–16.

LLNL (2022). "Downscaled CMIP3 and CMIP5 Climate and Hydrology Projections, <https://gdo-dcp.ucllnl.org>.

Lukas, J. J. and Payton, E. (2020). *Colorado River Basin climate and hydrology: State of the science*. Western Water Assessment, University of Colorado Boulder.

Meinshausen, M., Nicholls, Z. R., Lewis, J., Gidden, M. J., Vogel, E., Freund, M., Beyerle, U., Gessner, C., Nauels, A., Bauer, N., Canadell, J. G., Daniel, J. S., John, A., Krummel, P. B., Luderer, G., Meinshausen, N., Montzka, S. A., Rayner, P. J., Reimann, S., Smith, S. J., Van Den Berg, M., Velders, G. J., Vollmer, M. K., and Wang, R. H. (2020). "The shared socio-economic pathway (SSP) greenhouse gas concentrations and their extensions to 2500." *Geoscientific Model Development*, 13(8), 3571–3605.

Meinshausen, M., Smith, S. J., Calvin, K., Daniel, J. S., Kainuma, M. L., Lamarque, J., Matsumoto, K., Montzka, S. A., Raper, S. C., Riahi, K., Thomson, A., Velders, G. J., and van Vuuren, D. P. (2011). "The RCP greenhouse gas concentrations and their extensions from 1765 to 2300." *Climatic Change*, 109(1), 213–241.

NOAA (2022). "Climate at A Glance, <https://www.ncei.noaa.gov/access/monitoring/climate-at-a-glance/>.

Nocedal, J. and Wright, S. (2006). *Numerical optimization*. Springer Science.

Pierce, D. W., Cayan, D. R., and Thrasher, B. L. (2014). "Statistical Downscaling Using Localized Constructed Analogs (LOCA)." *Journal of Hydrometeorology*, 15(6), 2558–2585.

Ribes, A., Qasmi, S., and Gillett, N. P. (2021). "Making climate projections conditional on historical observations." *Science Advances*, 7(4), 1–10.

Smith, C., Hall, B., Dentener, F., Ahn, J., Collins, W., Jones, C., Meinshausen, M., Dlugokencky, E., Keeling, R., Krummel, P., Mühle, J., Nicholls, Z., and Simpson, I. (2021). "IPCC Working Group 1 (WG1) Sixth Assessment Report (AR6) Annex III Extended Data.

Tebaldi, C. and Arblaster, J. M. (2014). "Pattern scaling: Its strengths and limitations, and an update on the latest model simulations." *Climatic Change*, 122(3), 459–471.

Vano, J. A. and Lettenmaier, D. P. (2014). "A sensitivity-based approach to evaluating future changes in Colorado River discharge." *Climatic change*, 122(4), 621–634.

Wheeler, K. G., Udall, B., Wang, J., Kuhn, E., Salehabadi, H., and Schmidt, J. C. (2022). "What will it take to stabilize the Colorado River?." *Science*, 377(6604), 373–375.